Journal of Alloys and Compounds 621 (2015) 256–262

Contents lists available at ScienceDirect

Journal of Alloys and Compounds

journal homepage: www.elsevier.com/locate/jalcom

Phase transition, dielectric and piezoelectric properties of $Li_xK_{1-x}NbO_3$

R. Machado [a], A. Di Loreto [a,b], A. Frattini [a,b], M. Sepliarsky [a], O. de Sanctis [a], M.G. Stachiotti [a,*]

[a] Instituto de Física Rosario, Universidad Nacional de Rosario, 27 de Febrero 210 Bis, 2000 Rosario, Argentina
[b] Área Física, Dpto. de Química Física, FCByF, Universidad Nacional de Rosario, 2000 Rosario, Argentina

ARTICLE INFO

Article history:
Received 11 September 2014
Accepted 26 September 2014
Available online 5 October 2014

Keywords:
Ferroelectrics
Perovskites
Atomistic simulations

ABSTRACT

The influence of Li impurities on the phase transition, dielectric and piezoelectric properties of $KNbO_3$ ceramics is investigated. We found that Li doping alters the transition temperatures of $KNbO_3$. While the temperature for the orthorhombic–tetragonal phase transition decreases, the temperature of the cubic–tetragonal ferroelectric phase transition increases. The dielectric and piezoelectric properties of the ceramics are improved by the addition of Li. The experiments were contrasted and complemented with first-principles-based atomic level simulations to gain more insight into the intrinsic properties of the solid solution. We show that the impurities improve the dielectric properties due to a relaxational contribution of the off-center Li ions. The increase of the piezoelectric response is associated to the concentration dependence of the shear piezoelectric coefficients.

1. Introduction

Random lattice disorder produced by chemical substitution in ABO_3 perovskites can lead to the formation of dipolar impurities and defects that influence the properties of these materials. A prototypical case is that of Li ions substituting for K in the quantum paraelectric $KTaO_3$. On substituting at the K^+ site, the much smaller Li^+ ion occupies an off-center position with a displacement as large as a quarter of the lattice constant [1–3]. The resulting dipole moment is the precursor for the formation of polar nanoregions [4]. In this way, depending on the Li content, various phases from dipole glasslike to ferroelectric ones can be realized. Two review papers [5,6] reported the development of research in this material up to the early nineties and, since then, $Li_xK_{1-x}TaO_3$ continued to be a subject of numerous investigations. In contrast, the impact of Li doping on the properties of $KNbO_3$ has been much less investigated. Unlike $KTaO_3$, $KNbO_3$ is a ferroelectric with a strong remnant polarization, and off-center impurities may be coupled with the lattice polarization in a non-trivial way. Recent atomic level simulations [7] have shown however that an isolated lithium impurity in a $KNbO_3$ ferroelectric matrix takes off-center positions along [001] orientations, similar to the case of $Li_xK_{1-x}TaO_3$.

Besides its basic interest, the investigation of off-center impurities on systems undergoing structural phase transitions is a relevant topic to provide a better undestanding of lead-free piezoelectric materials [8]. It was shown, for example, that the addition of an appropriate amount of Li ions into a ferroelectric $Na_{0.5}K_{0.5}NbO_3$ matrix produces the enhancement of its piezoelectric properties. In that system, the role of off-center impurities seems to be crucial, being responsible for the formation of a structural instability at room temperature [9].

The above discussions highlight the need to investigate the role played by off-center impurities in the structural and electrical properties of a ferroelectric material. $KNbO_3$ is a prototypical ferroelectric material whose phase transitions have been studied in detail. It exhibits the same sequence of phase transitions as $Na_{0.5}K_{0.5}NbO_3$ or $BaTiO_3$, transforming from the cubic (C) paraelectric to the tetragonal (T) phase at 435 °C, from the tetragonal to the orthorhombic (O) phase at 225 °C and from the orthorhombic to the rhombohedral (R) phase at −10 °C. The T, O and R phases are all ferroelectrics. In most cases, however, the interest and success in $KNbO_3$ have been limited to single crystals, since the synthesis of dense and stoichiometric $KNbO_3$ ceramics has been difficult due to the formation of unstable secondary phases which show deliquescence when exposed to humidity [10,11]. In this paper we investigate the influence of Li impurities on the dielectric, piezoelectric and phase transition properties of $KNbO_3$ ceramics. We found that the Li doping shifts the transition temperatures producing an increase of the temperature range of stability of the tetragonal phase with increasing Li content. We also show that the off-center impurities improve the dielectric and piezoelectric properties of the ceramics. The experiments were complemented with computer simulations using an atomistic model with parameters fitted to first-principles calculations.

* Corresponding author.

http://dx.doi.org/10.1016/j.jallcom.2014.09.212
0925-8388/

2. Experimental procedure

$Li_xK_{1-x}NbO_3$ powders were synthesized from a mixture of Li_2CO_3, K_2CO_3 and Nb_2O_5 by a high-energy milling process using a planetary ball mill equipment (Torrey Hills Technologies ND 0.4 L). The carbonates are hygroscopic materials and hence due care was taken in their handling during the material formation [12]. The precursor powders were initially dried at 220 °C for 4 h to remove the absorbed moisture and then they were weighed based on the stoichiometric formula and milled for 24 h at 700 rpm. The milled powder was calcined at 700 °C for 4 h. The resulting powders were ball milled again for 24 h. The whole ball milling process was done in dry conditions, i.e. without the addition of a solvent in the milling jar, using nitrogen atmosphere to avoid humidity absorption. The obtained powders were pressed into disk-shape pellets 10 mm in diameter. The pellets were sintered at 1020 °C for 2 h. The density, measured by the Archimedés technique, reached up to 93% of the theoretical value. Crystal structure was analysed by X-ray diffraction (XRD) using a Philips X'Pert Pro X-ray diffractometer. For electrical studies, silver electrodes were sputtered on both sides of the samples. The temperature dependence of the dielectric properties of the ceramics was measured from 1 kHz to 2 MHz using an LCR meter (QuadTech 7600 plus) attached to a programmable furnace. The electric poling of the samples was performed at 120 °C in a silicone oil bath by applying a dc field of 3000 V/mm for 30 min. The electric field was maintained during cooling. The piezoelectric constant d_{33} was measured by a Berlincourt-type d_{33} meter (KCF technologies, model PM3001). The planar electromechanical coupling factor k_p was determined by the resonance–antiresonance method with the impedance analyser. All measurements were done within seven days after producing the pellets. This is because of the aging of the material, which was accelerated by the humidity absorption [10,11].

3. Atomistic model for $Li_xK_{1-x}NbO_3$

We consider in this work an interatomic potential approach based on a shell model, where the electronic polarization of the atoms is implemented via the Dick–Overhauser model [13,14], in which an atom is considered as a charged core connected to a massless charged shell. The equilibrium distance between the core and shell is a representation of the electronic polarization of that atom. The interactions between different atoms are represented by interatomic potentials whose parameters are fitted to achieve the best possible agreement with ab initio calculations.

The model contains fourth-order core–shell couplings (k_2 k_4), long-range coulombic interactions and short-range interactions described by two different types of potentials. A Born–Mayer potential $V = A\ e^{-r/\rho}$ is used for the K–O, Li–O, and Nb–O pairs, and a Buckingham potential $V(r) = A\ e^{-r/\rho} + C/r^6$ is used for O–O interactions. The model parameters for $KNbO_3$ were fitted in a previous work [15].

As we are interested in the simulation of $Li_xK_{1-x}NbO_3$ solid solutions, a Li–O interatomic potential was developed. This potential is compatible with the $KNbO_3$ model in that for simulating the alloy the possible difference between the two A-site ions lies in the different K–O and Li–O interactions and the different polarizability parameters for K and Li. The Li–O potential was obtained by adjusting its parameters to reproduce the energetics of Li off-center displacements in $KNbO_3$ calculated from ab initio calculations [7]. The resulting parameters for the Li–O Born–Mayer potential obtained from the fitting are $A = 3571.876$ eV and $\rho = 0.211417$ Å, while the polarizability parameter for Li is $k_2 = 500$ eV/Å^2. We note that the fitted Li–O potential when combined with the Nb–O and O–O parameters reproduces well the structural properties of $LiNbO_3$ [7]. That result improves the confidence in the Li–O potential for the modeling of $Li_xK_{1-x}NbO_3$ solid solutions.

The phase transition sequence and several finite-temperature properties of the material are investigated by molecular-dynamics (MD) simulations using the DL-POLY package [16]. The runs were performed employing a Hoover constant-(σ, T) algorithm with external stress set to zero; all cell lengths and cell angles were allowed to fluctuate. The simulations were performed randomly distributing Li impurities in a $10 \times 10 \times 10$ supercell (5000 atoms) with periodic boundary conditions. The time step was 0.4 fs, which provided enough accuracy for the integration of the shell coordinates. The total time of each simulation, after 5 ps of thermalization, was 45 ps.

4. Results and discussion

Fig. 1 shows the X-ray diffraction patterns of $Li_xK_{1-x}NbO_3$ ceramics at various concentrations ($x = 0$; 0.02; 0.04, and 0.06). It is seen that the recorded patterns matches very well with those of the orthorhombic structure corresponding to the JCPDF No 32-0822, which indicates that the sintered samples exhibit a single phase. The lattice parameters for pure $KNbO_3$, calculated using standard software, are $a = 5.7018$ Å, $b = 5.6936$ Å, and $c = 3.9822$ Å. No discernible difference in lattice parameters was observed among different Li concentrations.

The temperature dependence of dielectric constant for the $Li_xK_{1-x}NbO_3$ ceramic samples is shown in Fig. 2(real (a) and imaginary (b) parts). The data were taken during the cooling process of the thermal cycle. Although we did measurements at 10 different frequencies, only the data for 100 kHz are presented for the sake of clarity. The dielectric constants show well defined anomalies. The undoped $KNbO_3$ system exhibits the two typical phase transition peaks: the first associated with the O–T phase transition at 213 °C, while the second with the T–C phase transition at 420 °C. The dielectric constant reaches a value of approximately 470 at the T–C peak. It is clear from the figures that the addition of Li impurities not only increases the dielectric constant of the samples but also modifies the transition temperatures. While the Curie temperature increases with Li content, the peak associated with the O–T phase transition shifts to lower temperatures. The transition temperatures observed for the different Li concentrations are summarized in Table 1. We note that the temperature shifts produce an increase of the temperature range of stability of the tetragonal phase with increasing Li content. We have not measured the effects of Li impurities on the low-temperature R–O transition. Studies regarding that point were performed using the Raman scattering technique, and the results indicated that the phase transition of $Li_{0.01}K_{0.09}NbO_3$ is lower than that of pure $KNbO_3$ by 60 °C [17].

The piezoelectric d_{33} constants of poled ceramics measured by a Berlincourt-type d_{33} meter are given in Table 1. A value of 74 pC/N is obtained for the $KNbO_3$ sample, which is similar to other values reported in the literature [18,19]. We see that the addition of a 2% of Li impurities slightly increases d_{33} to 82 pC/N, while it remains unchanged for 4% of Li. A further increase of Li to 6% produces a worsening of the d_{33} piezoelectric constant. A similar concentration-dependent behavior is observed for the planar electromechanical coupling factor k_p.

To gain more insight into the results reported for the ceramics, we contrast and complement them with computer simulations using an atomistic model with parameters fitted to first-principles

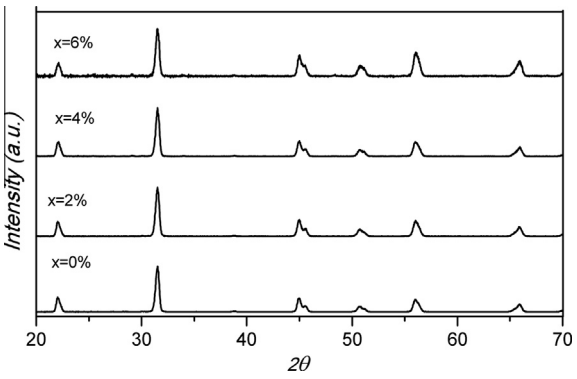

Fig. 1. XRD patterns of $Li_xK_{1-x}NbO_3$ ceramics ($x = 0.0$, 0.2, 0.4 and 0.6).

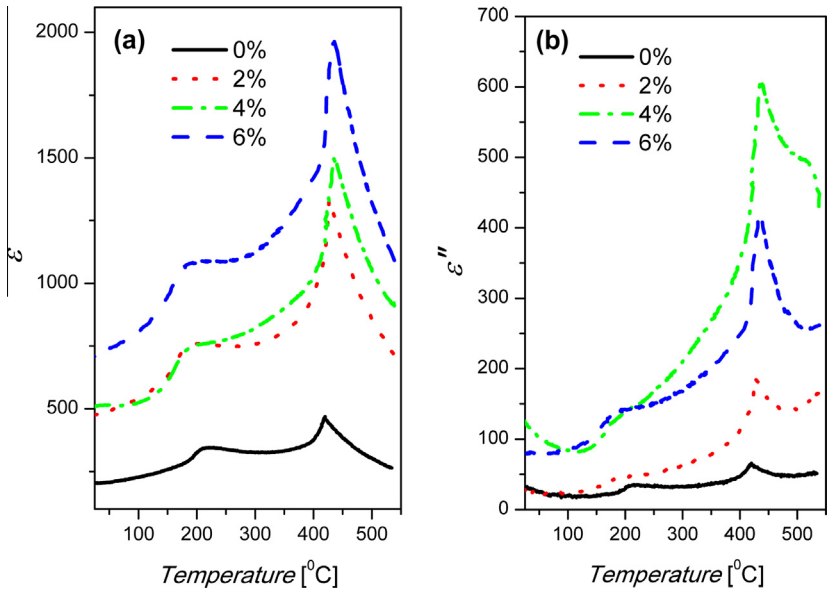

Fig. 2. Temperature dependence of the dielectric constant of $Li_xK_{1-x}NbO_3$ ceramics measured at 100 kHz: (a) real part and (b) imaginary part.

Table 1
Experimentally determined orthorhombic–tetragonal (O–T) and tetragonal–cubic (T-C) transition temperatures, piezoelectric constants (d_{33}) and planar electromechanical coupling factors (k_p) for $Li_xK_{1-x}NbO_3$ ceramics.

Li content (%)	T_{O-T} (°C)	T_{T-C} (°C)	d_{33} (pC/N)	k_p
0	213	420	74	0.30
2	189	427	82	0.32
4	186	434	81	0.32
6	182	435	40	0.27

calculations. That is, no explicit experimental data have been used as input to develop the model. The shell model for $KNbO_3$ used in this work correctly reproduces the temperature-driven phase transition sequence of the bulk [20]. Table 2 shows that an excellent overall agreement is obtained for the structural parameters, showing that the model reproduces the delicate structural changes involved in the transitions. The lattice parameters obtained from the model in the four phases agree with experimental values to better than 1%, and the calculated polarizations are in reasonably agreement with the experimental ones. Although the phase transition sequence is correctly reproduced, the theoretically determined transition temperatures tend to be too small compared with experiments (similar features are obtained in other systems with LDA-based models [15]. For that reason the results are presented here using a rescaled temperature to match the experimental Curie temperature. Table 2 shows that if the Curie temperature is rescaled to match the experimental value, the R–O and O–T transition temperatures are very close to the experimental values. It is worth mentioning that our model for $KNbO_3$ has been used successfully to reproduce the ferroelectric behavior of $KTa_xNb_{1-x}O_3$ solid solutions [20].

Table 2
Transition temperatures, structural parameters, and spontaneous polarization for the different phases of $KNbO_3$.

Parameter	MD simulations	Experiment
Rhombohedral		
a (Å)	4.042	4.016 [21]
θ (deg)	89.42	89.81
P(μC/cm^2)	46	
T_{R-O}(C°)	−8	−10
Orthorhombic		
a (Å)	4.071	4.037 [22]
$b = c$ (Å)	3.985	3.971
θ (deg)	90.70	90.15
P(μC/cm^2)	43	41 [23]
T_{O-T}(C°)	197	225
Tetragonal		
a (Å)	4.023	4.005 [24]
c (Å)	4.108	4.062
P (μC/cm^2)	33	30
T_{T-C} (C°)	435	435
Cubic		
a (Å)	4.062	4.025 [22]

As we are interested in the simulation of $Li_xK_{1-x}NbO_3$ solid solutions, a Li–O interatomic potential was developed based on the off-center behavior of an isolated Li impurity. We have recently investigated the tendency of a Li ion to move off-center in $KNbO_3$ [7]. That study clearly indicate that the impurity has a strong tendency to off-centering, with energy gains of 49 meV, 23 meV and 20 meV for the [0 0 1], [0 1 1] and [1 1 1] directions, respectively. The magnitude of the displacements along the three directions are 0.80 Å, 0.56 Å and 0.52 Å. So, like in $KTaO_3$, Li ions in $KNbO_3$ form reorientable dipoles which can influence the dielectric response of the system, as we will show later. In this way, a new Li–O potential was obtained by adjusting its parameters to reproduce the energetics of Li off-center displacements [7].

Fig. 3 shows the effect of the replacement of K by Li ions on the phase transition behavior of $K_{1-x}Li_xNbO_3$ solid solutions obtained from MD simulations. We have included in that figure the transition temperatures determined for the ceramics. The phase diagram clearly shows that Li impurities produce a decrease in the R–O and O–T transition temperatures while the Curie temperature increases, in qualitative agreement with the experimental results showed previously. It can be seen that the model displays stronger variations with Li concentration in comparison with the experimental data. As a consequence, the simulations predict a structural instability at room temperature (i.e. the presence of an O–T polymorphic phase transition at $x = 4.5\%$) increasing the piezoelectric response [25]. Since this instability was not observed in the ceramics, hereafter we will present the theoretical results only for $x < 4\%$. For completeness, we present in Table 3 the resulting lattice

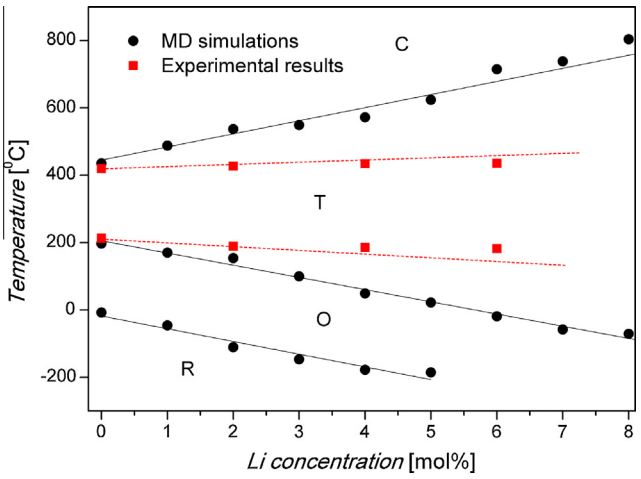

Fig. 3. Phase diagram of $Li_xK_{1-x}NbO_3$ resulting from the MD simulations (black circles). The results are presented using a rescaled temperature to match the Curie temperature determined for the ceramics. The experimentally determined transition temperatures are indicated by red squares. (For interpretation of the references to color in this figure legend, the reader is referred to the web version of this article.)

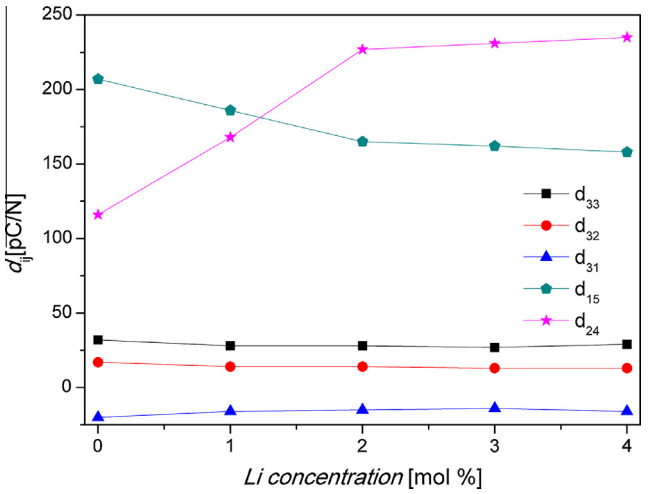

Fig. 4. Concentration dependence of piezoelectric coefficients d_{ij} for $Li_xK_{1-x}NbO_3$. While the longitudinal and transverse coefficients practically do not depend on Li content, the shear components present quite strong concentration dependence for $x < 2\%$.

constants as a function of Li content for the different phases at four selected temperatures. It is clear that the impurities reduce the lattice constants in all phases. We were not able to detect that effect from the X-ray diffraction patterns showed in Fig. 1. The only exception is for the lattice constant c of the tetragonal phase, which increases with content of Li. This can be understood because Li ions in the tetragonal phase are all off-center along the [001] direction. So, they have their local dipole moments always parallel to the macroscopic polarization, without hopping to another off-center position [7]. As the local polarization of Li is stronger than the one for $KNbO_3$, the impurities reinforce the average macroscopic polarization of the material (see Table 3) and an increment of the tetragonal strain can be expected. However, as seen in all the other phases, the unit-cell volume shrinks with the addition of Li.

To provide microscopic insights into the field-induced properties, we have determined the dielectric and piezoelectric coefficients of the $K_{1-x}Li_xNbO_3$ solid solutions at room temperature by calculating the change in the polarization and the elastic strain of the crystal under an applied electric field. In the orthorhombic phase the polarization of the material is along the [011] cubic direction. For our calculations we used an orthorhombic coordinate system where $[100]^o = [100]^c$, $[010]^o = [01-1]^c$, and $[001]^o = [011]^c$. The superscripts o and c stands for orthorhombic and cubic respectively. From symmetry considerations, there are five independent piezoelectric coefficients for the orthorhombic phase: the longitudinal d_{33}, the transverse d_{31} and d_{32}, and the shear components d_{15} and d_{24}. The dielectric tensor is diagonal in the orthorhombic coordinate system.

Fig. 4 shows the Li concentration dependence of the piezoelectric coefficients at room temperature. The theoretical values for pure $KNbO_3$ are $d_{31} = -20$, $d_{32} = 17$, $d_{33} = 32$, $d_{15} = 207$, and $d_{24} = 116$ pC/N, which are in reasonable good agreement with reported experimental data for single crystals [26,27,28]. It is observed that the longitudinal and transverse coefficients do not depend on Li content. On the contrary, the shear components present concentration dependence. At low Li concentrations ($x < 2\%$), the impurities strongly affect both shear components, d_{24} increases while d_{15} decreases with x. This impurity effect seems to saturate and the shear components remain practically constants for $2\% < x < 4\%$. To better compare the theoretical results with the experimental measurements, we determined the maximum deformation of the system along the direction of an external electric field. This value was calculated by the longitudinal piezoelectric coefficient in an arbitrary direction, $d_{33}^*(\varphi, \theta, \psi)$, where φ, θ

Table 3
Lattice parameters, cell volume and spontaneous polarizations of $Li_xK_{1-x}NbO_3$ solid solutions at different temperatures obtained from MD simulations.

Phase	T (°C)		0%	1%	2%	3%	4%
R	−245	a (Å)	4.0309	4.0306	4.0302	4.0297	4.0290
		α (degrees)	89.37	89.34	89.33	89.33	89.37
		V (Å^3)	65.48	65.47	65.45	65.42	65.39
		P (μC/cm^2)	46.26	46.75	46.95	47.27	47.30
O	25	a (Å)	3.9852	3.9843	3.9836	3.9827	3.9835
		c (Å)	4.0713	4.0713	4.0710	4.0706	4.0692
		β (degrees)	89.30	89.28	89.26	89.24	89.24
		V (Å^3)	66.05	66.04	66.01	65.99	65.95
		P (μC/cm^2)	43.46	43.89	44.24	44.70	44.77
T	370	a (Å)	4.0236	4.0209	4.0187	4.0166	4.0149
		c (Å)	4.1082	4.1138	4.1179	4.1211	4.1235
		V (Å^3)	66.51	66.51	66.50	66.48	66.47
		P (μC/cm^2)	33.25	34.66	36.00	36.73	37.28
C	735	a (Å)	4.0574	4.0567	4.0558	4.0553	4.0548
		V (Å^3)	66.80	66.76	66.72	66.69	66.67

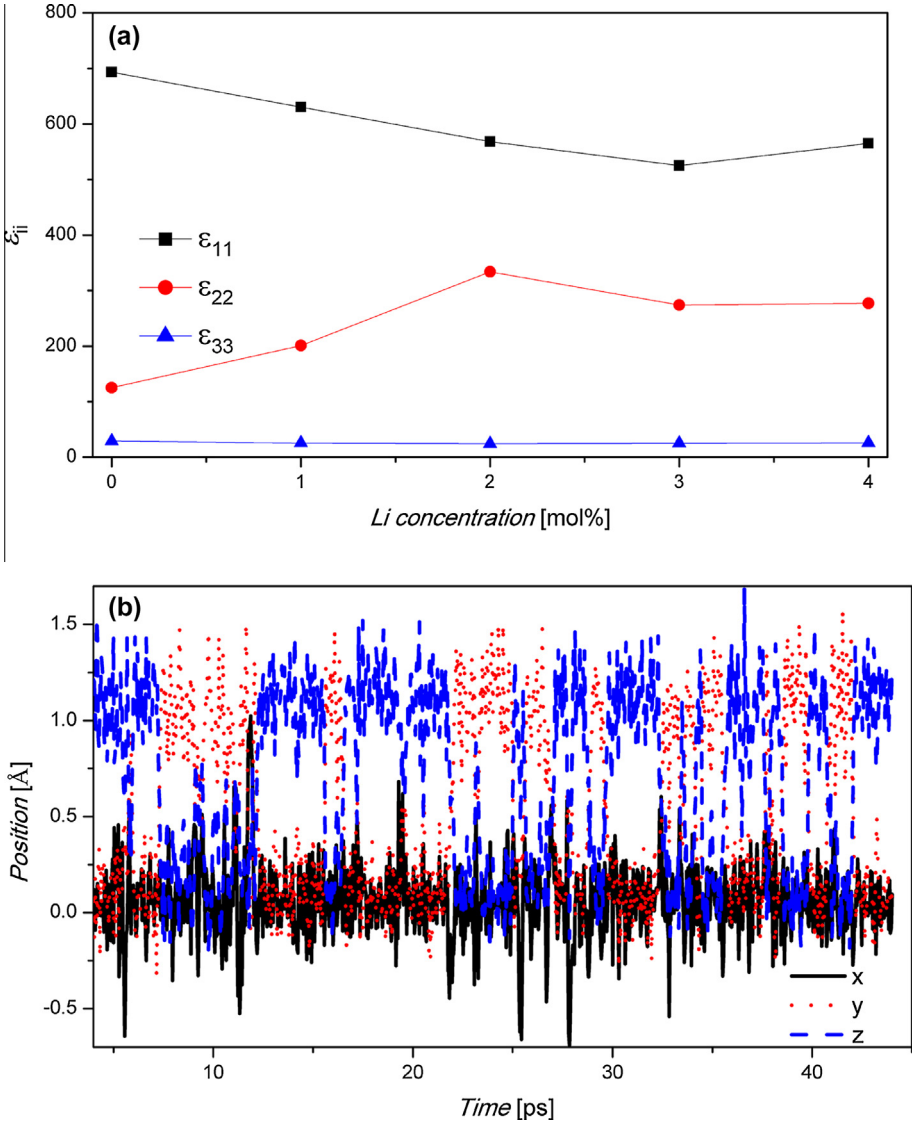

Fig. 5. (a) Concentration dependence of dielectric coefficients ε_{ij} for $Li_xK_{1-x}NbO_3$. (b) Time evolution of off-center displacements for an arbitrary chosen Li ion in the orthorhombic phase. Each cartesian component is plotted with a different color and style. (For interpretation of the references to color in this figure legend, the reader is referred to the web version of this article.)

are ψ are the Euler angles. In the orthorhombic phase $d_{33}^*(\varphi,\ \theta) = \cos(\theta)[(d_{15} + d_{31})\ \sin^2(\theta)\sin^2(\varphi) + (d_{24} + d_{32})\sin^2(\theta)\cos^2(\varphi) + d_{33}\cos^2(\theta)]$, and its maximum occurs at $\varphi = 0°$ or $\varphi = 90°$. Values of d_{33}^* of 78, 97 and 100 pC/N were obtained for $x = 0$, 0.02 and 0.04 respectively. As seen, there is quite good qualitative agreement between those values and the experimental d_{33} coefficients reported in Table 1. In both cases there are increments of d_{33} for the material doped with 2% of Li, while the coefficient remains practically unchanged for $x = 4\%$. Our simulations illustrate that this behavior is originated from the concentration dependence of the shear coefficients.

Fig. 5a shows the Li concentration dependence of the dielectric tensor at room temperature obtained from the MD simulations. It can be seen that the behavior of ε_{33}, ε_{22} and ε_{11} with x resembles the ones reported previously for d_{33}, d_{24} and d_{15} respectively. The increment of d_{24} and ε_{22} reflects the dielectric softening of the material along the $[0\,1\,0]^\circ$ direction induced by the Li doping. A similar softening was observed in $KNbO_3$ and $BaTiO_3$ single crystals but in those cases the behavior was driven by temperature-driven phase transitions [29,30]. We note that it would not be correct to compare the MD results with the experimental data of the dielectric behavior reported previously. The theoretical dielectric constants were obtained as response to a static electric field, while the sinterized ceramics showed important losses in the low-frequency range due to the high conductivity of the samples [31,32].

To better understand the role played by the Li impurities in the dielectric behavior, we show in Fig. 5b the local dynamics of an arbitrarily chosen Li in the orthorhombic phase. The figure displays the time evolution of the Cartesian coordinates of the ion from its ideal perovskite A-site. The Li impurity clearly displays a relaxation dynamics between $[0\,0\,1]^c$ off-center positions. This behavior resembles the case of Li in $KTaO_3$, where the low-temperature freezing of the relaxation dynamics produces a dipole-glass phase. There is however one important difference. While in $KTaO_3$ the impurity jumps between six equivalent off-center positions, the macroscopic polarization of $KNbO_3$ favors only two of the six possibilities. That is, if the orthorhombic phase is polarized along the $[0{+}1{+}1]^c$ direction, Li ions relax only between $[0\,0{+}1]^c$ and $[0{+}1\,0]^c$ off-center positions, being forbidden the other four directions for off-centering. This off-center relaxational dynamics origi-

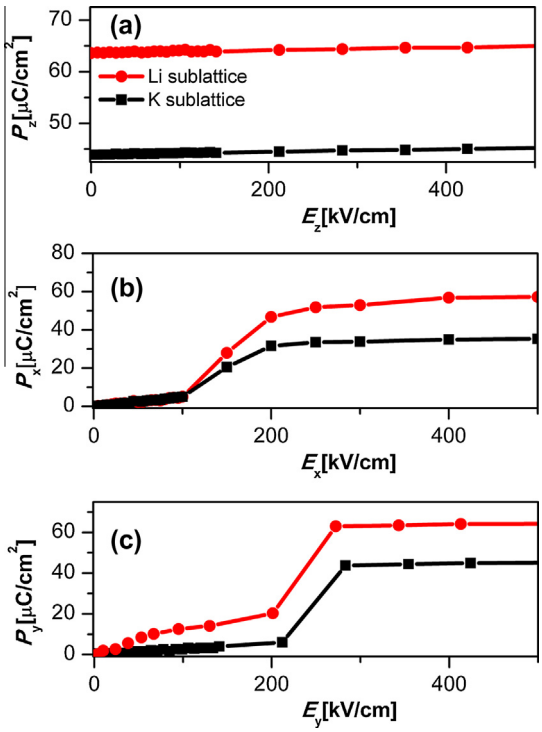

Fig. 6. Field-induced polarization of the Li and K sublattices as a function of the field intensity for the case $x = 2\%$. The electric field is applied along the three axes of the orthorhombic system: (a) $[001]^{\circ} = [011]^{c}$, (b) $[100]^{\circ} = [100]^{c}$, and (c) $[010]^{\circ} = [01\text{-}1]^{c}$.

nates the dielectric response showed in Fig. 5a. To better visualize that point, we have performed a microscopic characterization in terms of local polarizations, distinguishing unit cells centered on Li and K ions. Fig. 6 shows the field-induced polarizations of the Li and K sublattices as a function of the applied electric field along the three axes of the orthorhombic system. Fig. 6a shows the case for an electric field applied along the polar direction ($[001]^{\circ} = [011]^{c}$). It is clear that although the polarization of the Li sublattice is greater, the slope of the response of the two sublattices is practically the same. In this case the Li relaxational dynamics is not altered by the presence of the electric field and the Li ions occupy [00+1]c and $[0+10]^{c}$ off-center positions with equal probability. This explains why the dielectric constant ε_{33} does not depend on Li content. When the electric field is applied along the $[100]^{c}$ direction (Fig. 6b), the Li relaxational dynamics seems to delay the response, producing a dielectric hardening of the material. This explains the slight decrease of ε_{11} with Li content observed in Fig. 5. A quite different response of the two sublattices is observed however when the electric field is applied along the $[01\text{-}1]^{c}$ direction (Fig. 6c). In that case, the Li relaxational dynamics is modified in such way that the probability of occupation of the $[0+10]^{c}$ off-center position is greater than $[00+1]^{c}$, thereby increasing the polarization response along the orthorhombic y axis. This explains why the dielectric constant ε_{22} increases with Li content.

5. Conclusions

$Li_xK_{1-x}NbO_3$ ($x = 0$, 0.2,0,4 and 0.6) pellets were obtained via ordinary high-energy ball milling process. All the samples exhibited an orthorhombic single phase. Dielectric and piezoelectric measurements were performed and the results were complemented with computer simulations using a first-principles-based atomistic model.

We found that the Li doping shifts the transition temperatures producing an increase of the temperature range of stability of the tetragonal phase with increasing Li content. We show that a small amount of Li (2%) increases the piezoelectric d_{33} coefficient and the planar electromechanical coupling factor of the ceramics. We have associated that behavior to a strong concentration dependence of the shear coefficients obtained from the simulations of the solid solution. We also show that the impurities improve the dielectric properties due to a relaxational contribution of the off-center Li ions.

Acknowledgments

We acknowledge computing time at the CCT-Rosario Computational Center. This work was sponsored by Consejo Nacional de Investigaciones Científicas y Tecnológicas (CONICET) and Agencia Nacional *de Promoción Científica y Tecnológica (ANPCyT) de la República Argentina*. MGS thanks support from Consejo de Investigaciones de la Universidad Nacional de Rosario (CIUNR).

References

[1] J. van der Klink, F. Borsa, NMR study of the quasi-reorientational dynamics of Li ions in $KTaO_3$:Li, Phys. Rev. B 30 (1984) 52–64.
[2] M.G. Stachiotti, R.L. Migoni, Lattice polarisation around off-centre Li in $Li_xK_{1-x}TaO_3$, J. Phys. Condens. Matter. 2 (1990) 4341–4350.
[3] R.I. Eglitis, A.V. Postnikov, G. Borstel, Semiempirical Hartree–Fock calculations for pure and Li-doped $KTaO_3$, Phys. Rev. B 55 (1997) 12976–12981.
[4] M.G. Stachiotti, R.L. Migoni, U.T. Höchli, The validity of the non-linear shell model for localized dipole moments in $Li_xK_{1-x}TaO_3$, J. Phys. Condens. Matter. 3 (1991) 3689.
[5] U.T. Höchli, K. Knorr, A. Loidl, Orientational glasses, Adv. Phys. 39 (1990) 405–615.
[6] B. Vugmeister, M. Glinchuk, Dipole glass and ferroelectricity in random-site electric dipole systems, Rev. Mod. Phys. 62 (1990) 993–1026.
[7] R. Machado, M. Sepliarsky, M.G. Stachiotti, Off-center impurities in a robust ferroelectric material: case of Li in $KNbO_3$, Phys. Rev. B 86 (2012) 094118.
[8] Y. Saito, H. Takao, T. Tani, T. Nonoyama, K. Takatori, T. Homma, et al., Lead-free piezoceramics, Nature 432 (2004) 84–87.
[9] Y. Guo, K. Kakimoto, H. Ohsato, Phase transitional behavior and piezoelectric properties of $(Na_{0.5}K_{0.5})NbO_3$–$LiNbO_3$ ceramics, Appl. Phys. Lett. 85 (2004) 4121.
[10] K. Kakimoto, I. Masuda, H. Ohsato, Lead-free $KNbO_3$ piezoceramics synthesized by pressure-less sintering, J. Eur. Ceram. Soc. 25 (2005) 2719–2722.
[11] H. Birol, D. Damjanovic, N. Setter, Preparation and characterization of $KNbO_3$ ceramics, J. Am. Ceram. Soc. 88 (2005) 1754–1759.
[12] T. Rojac, M. Kosec, M. Połomska, B. Hilczer, P. Šegedin, A. Bencan, Mechanochemical reaction in the K_2CO_3–Nb_2O_5 system, J. Eur. Ceram. Soc. 29 (2009) 2999–3006.
[13] B. Dick, A. Overhauser, Theory of the dielectric constants of alkali halide crystals, Phys. Rev. 112 (1958) 90–103.
[14] M. Sepliarsky, M.G. Stachiotti, R. Migoni, Structural instabilities in $KTaO_3$ and $KNbO_3$ described by the nonlinear oxygen polarizability model, Phys. Rev. B 52 (1995) 4044–4049.
[15] M. Sepliarsky, A. Asthagiri, S.R. Phillpot, M.G. Stachiotti, R.L. Migoni, Atomic-level simulation of ferroelectricity in oxide materials, Curr. Opin. Solid State Mater. Sci. 9 (2005) 107–113.
[16] I.T. Todorov, W. Smith, K. Trachenko, M.T. Dove, DL_POLY_3: new dimensions in molecular dynamics simulations via massive parallelism, J. Mater. Chem. 16 (2006) 1911.
[17] S.B. Dai, Y.D. Juang, J.S. Hwang, S.Y. Chu, Using Raman scattering to study the doping effect and low-temperature phase transition of $Li_{0.01}K_{0.99}NbO_3$ ceramics, J. Cryst. Growth. 257 (2003) 316–320.
[18] K. Matsumoto, Y. Hiruma, H. Nagata, T. Takenaka, Piezoelectric properties of pure and Mn-doped potassium niobate ferroelectric ceramics, Jpn. J. Appl. Phys. 45 (2006) 4479–4483.
[19] K. Hikita, Y. Hiruma, H. Nagata, T. Takenaka, Shear-mode piezoelectric properties of $KNbO_3$-based ferroelectric ceramics, Jpn. J. Appl. Phys. 48 (2009) 07GA05.
[20] M. Sepliarsky, S.R. Phillpot, D. Wolf, M.G. Stachiotti, R.L. Migoni, Atomic-level simulation of ferroelectricity in perovskite solid solutions, Appl. Phys. Lett. 76 (2000) 3986.
[21] A.W. Hewat, Cubic–tetragonal–orthorhombic–rhombohedral ferroelectric transitions in perovskite potassium niobate: neutron powder profile refinement of the structures, J. Phys. C Solid State Phys. 6 (1973) 2559–2572.
[22] G. Shirane, R. Newnham, R. Pepinsky, Dielectric properties and phase transitions of $NaNbO_3$ and $(Na, K)NbO_3$, Phys. Rev. 96 (1954) 581–588.
[23] P. Gunter, Spontaneous polarization and pyroelectric effect in $KNbO_3$, J. Appl. Phys. 48 (1977) 3475.

[24] S. Triebwasser, Behavior of ferroelectric $KNbO_3$ in the vicinity of the cubic–tetragonal transition, Phys. Rev. 101 (1956) 993–998.
[25] R. Machado, M. Sepliarsky, M.G. Stachiotti, Microscopic scale investigation of piezoelectric properties of lead-free alkaline niobates, Appl. Phys. Lett. 103 (2013) 242901.
[26] E. Wiesendanger, Dielectric, mechanical and optical properties of orthorhombic $KNbO_3$, Ferroelectrics 6 (1973) 263–281.
[27] P. Günter, Piezoelectric tensor of $KNbO_3$, Jpn. J. Appl. Phys. 16 (1977) 1727–1728.
[28] S. Wada, K. Muraoka, H. Kakemoto, T. Tsurumi, H. Kumagai, Enhanced piezoelectric properties of potassium niobate single crystals by domain engineering, Jpn. J. Appl. Phys. 43 (2004) 6692–6700.
[29] M. Budimir, D. Damjanovic, N. Setter, Piezoelectric anisotropy–phase transition relations in perovskite single crystals, J. Appl. Phys. 94 (2003) 6753.
[30] Linyun Liang, Y.L. Li, S.Y. Hu, Long-Qing Chen, Guang-Hong Lu, Piezoelectric anisotropy of a $KNbO_3$ single crystal, J. Appl. Phys. 108 (9) (2010) 094111.
[31] B. Sundarakannan, K. Kakimoto, H. Ohsato, Frequency and temperature dependent dielectric and conductivity behavior of $KNbO_3$ ceramics, J. Appl. Phys. 94 (2003) 5182.
[32] G. Singh, V.S. Tiwari, P.K. Gupta, Role of oxygen vacancies on relaxation and conduction behavior of $KNbO_3$ ceramic, J. Appl. Phys. 107 (2010) 064103.